Supplementary information

Enhancing Inverted Perovskite Solar Cells via Hydrophilic Surface Modification of NiO_x Using Aluminate Coupling Agents

Hanhong Zhang,[1,2,3]‡ Wenjing Hou,[1]‡ Yuanlong Deng,[3] Jun Song,[2]* Fan Zhang[1]*

[1]College of Physics and Optoelectronic Engineering & Qingdao Key Laboratory of Optics and Optoelectronics & Engineering Research Center of Advanced Marine Physical Instruments and Equipment/Ministry of Education, Ocean University of China, Qingdao, 266100, P. R. China

[2]Center for Biomedical Optics and Photonics (CBOP) & College of Physics and Optoelectronic Engineering, Key Lab of Optoelectronics Devices and Systems of Ministry of Education/Guangdong Province, Shenzhen University, Shenzhen, 518060, P. R. China

[3]Shenzhen City Polytechnic, Shenzhen, 518000, P. R. China

* Corresponding Author

‡ These authors contributed equally to this work.

E-mail: zf@ouc.edu.cn; songjun@szu.edu.cn

1. Materials

Nickel oxide (NiO_x) particles, [6,6]-phenyl-C61-butyric acid methyl ester ($PC_{61}BM$), 4,7-diphenyl-1,10-phenanthroline (Bphen) were obtained from Vizuchem (Shanghai). Aluminum di(isopropoxide)acetoacetic ester chelate (AL17, 97%) were procured from Huali Corp (China). Formamidine hydroiodide (FAI, 99.99%), Cesium iodide (CsI, 99.99%), Methylammonium bromine (MABr, 99.99%), Methylammonium Chlorine (MACl, 99.99%), Lead (II) bromide ($PbBr_2$, 99.99%), Lead (II) iodide (PbI_2, 99.99%) were all obtained from Advanced Electron Technology (China). All solvents used in this study were acquired from Sigma Aldrich. All materials were commercially sourced and used without additional treatment.

2. Devices fabrication

Small-size solar cell fabrication: The $FA_{0.83}Cs_{0.07}MA_{0.13}PbI_{2.64}Br_{0.39}$ precursor solution was prepared by dissolving FAI (285.5 mg), CsI (36.4 mg), MABr (29.1 mg), PbI_2 (802.1 mg), and $PbBr_2$ (95.42) in DMF (0.87 mL) and NMP (0.13 mL). To enhance the quality of the perovskite, 2 mg/mL PBAI was added to the precursor. The NiO_x precursor solution was prepared by dispersing nickel oxide particles in deionized water (20mg/mL).

The pre-patterned ITO glass substrates were cleaned by ultrasonication in deionized water, acetone, and isopropanol for 15 minutes each. Before use, the ITO was further cleaned with ultraviolet ozone for 15 minutes. The substrate was then spin-coated with NiO_x nanoparticle solution at 3000 rpm for 30 seconds and annealed in ambient air at 120 °C for 15 minutes. For the AL17-PSC, the NiO_x film was modified by spin-coating an AL17 solution (2 mg/mL in ethanol) onto the NiO_x film at 3000 rpm for 30 seconds. Clean the film with ethanol to leave the self-assembled monolayer (SAM), and then anneal at 120°C for 1 minutes to remove excess solvent. The perovskite precursor solution was deposited onto the ITO/NiO_x surface and spin-coated at 7000 rpm for 30 seconds. 2-Butanol (200 μL) was used as the anti-solvent at the 13th-14th second of the spin-coating process, followed by annealing at 100 °C for 30 minutes. Subsequently, 20 mg/mL PCBM was spin-coated at 1500 rpm

for 60 seconds, followed by 0.7 mg/mL Bphen spin-coated at 6000 rpm for 30 seconds. Finally, a 100 nm thick layer of Ag was thermally evaporated as an electrode using a shadow mask.

***Mini-module fabrication by spin-coating*:** Compared to the fabrication parameters of small-area solar cells, the only changes made were increasing the volume of the solutions and using a multi-channel pipette; all other parameters remained unchanged. Perovskite modules containing 10 series-connected sub-cells were fabricated on 5×5 cm^2 ITO glass substrates. The series interconnections of the modules were achieved through P1, P2, and P3 lines. The lines were patterned using a laser scribing system with a wavelength of 532 nm and a frequency of 50 kHz. The P1, P2, and P3 lines were scribed before cleaning the ITO substrates, as well as before and after electrode evaporation. The scribing parameters were 500 mm/s at 8.0 W for P1, 1000 mm/s at 0.8 W for P2, and 500 mm/s at 1.6 W for P3.

Mini-module fabrication by blade-coating: The $FA_{0.3}MA_{0.7}PbI_3$ precursor solution was prepared by dissolving FAI (36.1 mg), MAI (77.9 mg), MACl (5 mg) and PbI_2 (461 mg) in 2-Methoxyethanol (0.93 mL), DMF (0.02 mL) and NMP (0.05 mL). The perovskite films were fabricated via the blade-coating method, with a blade gap of 200 μm and a coating speed of 20 mm/s. After coating, the wet films underwent vacuum flash evaporation for 40 seconds, followed by annealing on a hot plate at 100 °C for 20 minutes. The remaining fabrication procedures were consistent with those used in the spin-coating method.

3. Measurements and characterizations

Photovoltaic performance measurement: Solar irradiation (AM 1.5G, 100 mW cm^{-2}) was simulated using a sun simulator (Zolix Sirius-SS, AAA). J-V curves were measured with a Keithley 2400 source meter, calibrated using a silicon photodiode (ABET technology). EQE curves were acquired using a QE-R quantum efficiency system (Enlitech). The full spectrum LED solar simulator was used to investigated the stability of the minimodule (SLS-LED-80).

Confocal laser-scanning fluorescence microscopy measurements: CLFM images were

performed using a Leica TCS SP8 STED 3X system equipped with an HC PL APO CS2 100×/1.40 OIL objective lens and a PicoHarp 300 time-correlated single-photon counting system. This setup facilitated point-by-point scanning, enabling arbitrary selection of bleaching regions and adjustable laser intensity and duration. A super-continuum visible laser (600 nm, 720 $\mu J \cdot cm^{-2}$ per pulse, 80 MHz) served as the excitation source for CLFM imaging. Emission fluorescence signals from perovskite films were detected using a hybrid detector (HyD SMD) for high-resolution CLFM images.

X-ray photoelectron spectroscopy (XPS) and Ultraviolet photoelectron spectroscopy (UPS) measurements: XPS measurements were conducted using a Thermo Scientific ESCALAB Xi+ with 150 W monochromated Al Kα (1486.68 eV) radiation under a base pressure of approximately 1×10^{-9} mbar. Energy referencing was performed using the hydrocarbon C1s line at 284.8 eV from adventitious carbon. UPS measurements were performed on a Thermo Scientific ESCALab 250Xi, where Valence band (VB) spectra were acquired using a monochromatic He I light source (21.2 eV) and a VG Scienta R4000 analyzer. A sample bias of −5 V was applied to observe the secondary electron cutoff (SEC), and the work function (ϕ) was determined by the difference between the photon energy and the binding energy of the secondary cutoff edge.

Fourier Transform Infrared Spectrometer (FTIR) and Transmission electron microscope (TEM) measurements: FTIR measurements were conducted using a Shimadzu IRTracer 100 from Japan. TEM measurements were performed on a JEOL JEM 2100 F from Japan. To examine the chemical bond changes between AL17 and NiO_x, we added 100 mg of NiO_x nanoparticles and 100 mg AL17 to 1 ml DMF. After ultrasonic treatment, followed by high-speed centrifugation and washing with DMF, we obtained NiO_x fully coated with AL17, which we define as NiO_x@AL17 nanoparticles. We used the NiO_x@AL17 nanoparticles for FTIR and TEM measurements.

Scanning Electron Microscope (SEM) and Atomic Force Microscope (AFM) measurements: SEM images were carried out on a Thermo Fisher Scientific-Quanta FEG 250. AFM images were

performed on a Bruker-Dimension Icon. KPFM measurements were performed on a SHIMADZU SPM-9700HT atomic force microscope.

Tables and Figures:

Table S1. The deconvoluted peaks of O 1s spectra as shown in Figures 2e and 2f.

Samples	Element	k factor	Absorption Correction	Wt%
NiO_x	O	1.84933	1.00	14.65
	Al	1.03388	1.00	0.20
	Ni	1.29836	1.00	85.15
NiO_x@AL17	O	1.84933	1.00	20.56
	Al	1.03388	1.00	0.00
	Ni	1.29836	1.00	79.44

Table S2. The deconvoluted peaks of O 1s spectra as shown in Figures 2e and 2f.

Samples	Component	Peaks (eV)	Area ratio (%)
NiO_x	Ni^{2+}–O	529.1	29.4
	Ni^{2+}–OH	530.9	35.5
	Ni^{3+}–O	532.1	28.1
	Ni^{4+}–O	533.3	7.0
NiO_x/AL17	Ni^{2+}–O	529.1	23.9
	Ni^{2+}–OH	530.8	32.5
	Ni^{3+}–O	532.2	37.3
	Ni^{4+}–O	533.5	6.2

Table S3. The deconvoluted peaks of Ni 2p spectra as shown in Figures 2g and 2h.

Samples	Component	Peaks (eV)	Area ratio (%)
NiO_x	Ni^{2+}	854.0	40.7
	Ni^{3+}	**855.6**	**43.5**
	Ni^{4+}	857.1	15.8
NiO_x/AL17	Ni^{2+}	853.7	39.9
	Ni^{3+}	**855.4**	**46.3**
	Ni^{4+}	857.1	13.8

Table S4. The deconvoluted peaks of Pb 4f and I 3d spectra as shown in Figures S9 and S10.

Samples	Component	Peaks (eV)	Area ratio (%)
NiO_x/Perovskite	Pb $4f_{5/2}$	142.9	38.5
	Pb $4f_{7/2}$	138.1	51.4
	Metal Pb 4f	141.2/136.2	11.1
	I $3d_{3/2}$	630.6	41.2
	I $3d_{5/2}$	619.1	58.8
	Pb:I		2.89
NiO_x/AL17/Perovskite	Pb $4f_{5/2}$	142.8	42.4
	Pb $4f_{7/2}$	137.9	53.7
	Metal Pb 4f	141.2/136.2	3.9
	I $3d_{3/2}$	630.5	40.7
	I $3d_{5/2}$	619.0	59.3
	Pb:I		3.01

Table S5. Energy-level parameters for the corresponding perovskite, NiO_x, and NiO_x/AL17 films.

Samples	**E_F (eV)**	**VBM (eV)**	**VB (eV)**
Perovskite	-4.61	-0.95	-5.56
NiO_x	-4.51	-0.57	-5.08
NiO_x/AL17	-4.48	-0.65	-5.13

Table S6. The PL lifetime parameters from the PL decay curves in Figure S13b.

Samples	τ_1 (ns)	$-A_1\tau_1/\Sigma A_x\tau_x$ (%)	τ_2 (ns)	$-A_2\tau_2/\Sigma A_x\tau_x$ (%)	τ_{ave} (ns)
NiO_x/Perovskite	0.73	83.2	2.63	16.8	1.04
NiO_x/AL17/Perovskite	0.75	64.9	6.04	35.1	2.61

Table S7. Photovoltaic parameters for the best-performing control, and AL17 PSCs.

Samples	Scan direction	V_{OC} (V)	J_{SC} (mA cm^{-2})	FF	PCE (%)
NiO_x	forward	1.092	23.41	0.791	20.24
	reverse	1.122	23.49	0.819	21.58
NiO_x/AL17	forward	1.206	23.53	0.836	23.75
	reverse	1.209	23.47	0.840	23.82

Table S8. Average PV parameters of the control and AL17 PSCs from 24 devices.

Styles	V_{OC} (V)	J_{SC} (mA cm^{-2})	FF	PCE (%)
Control	1.113±0.006	22.84±0.32	0.815±0.008	20.81±0.27
AL17	1.205±0.006	23.49±0.32	0.831±0.007	23.52±0.36

Table S9. Photovoltaic parameters of the champion control and AL17 modified PSCMs.

Styles	V_{OC} (V)	J_{SC} (mA cm^{-2})	FF	PCE (%)
Control	11.20	2.18	0.761	18.61
AL17	12.11	2.30	0.783	21.80

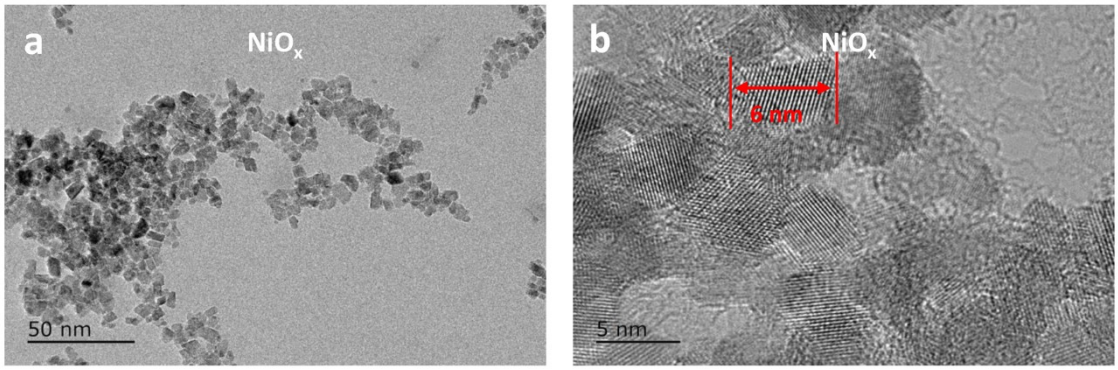

Figure S1. TEM images of NiO_x particles: (a) low magnification and (b) high magnification.

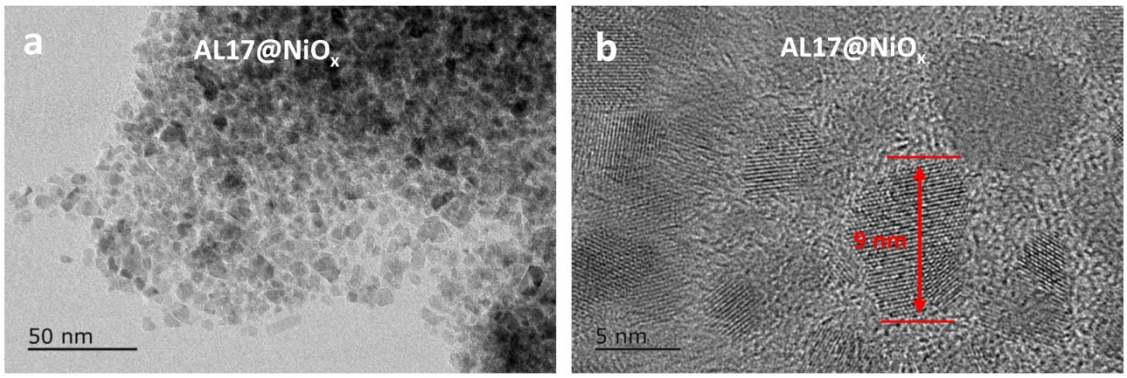

Figure S2. TEM images of NiO_x particles after AL17 coating: (a) low magnification and (b) high magnification.

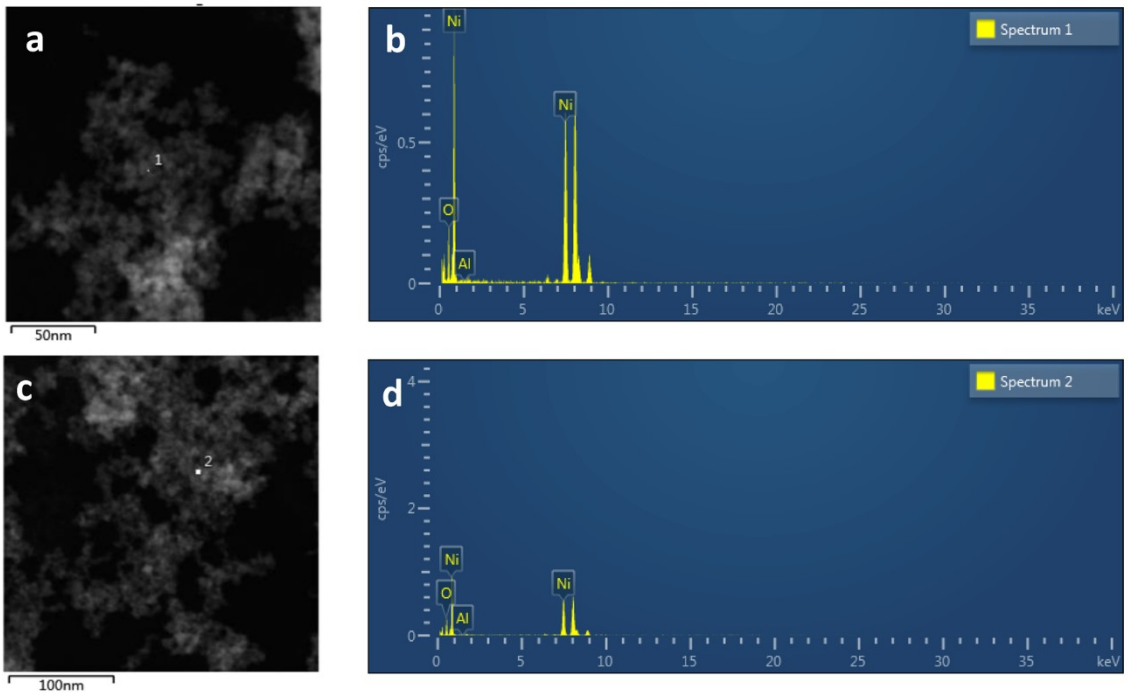

Figure S3. (a and b) TEM images and EDS spectrum of NiO_x nanoparticles after AL17 coating. (c and d) TEM images and EDS spectrum of NiO_x nanoparticles.

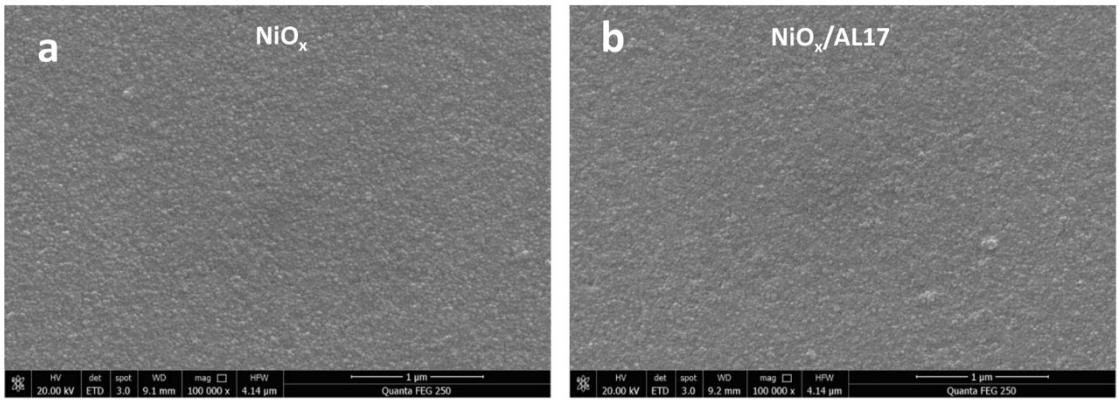

Figure S4. SEM images of NiO_x and NiO_x/AL17 surfaces prepared by spin-coating.

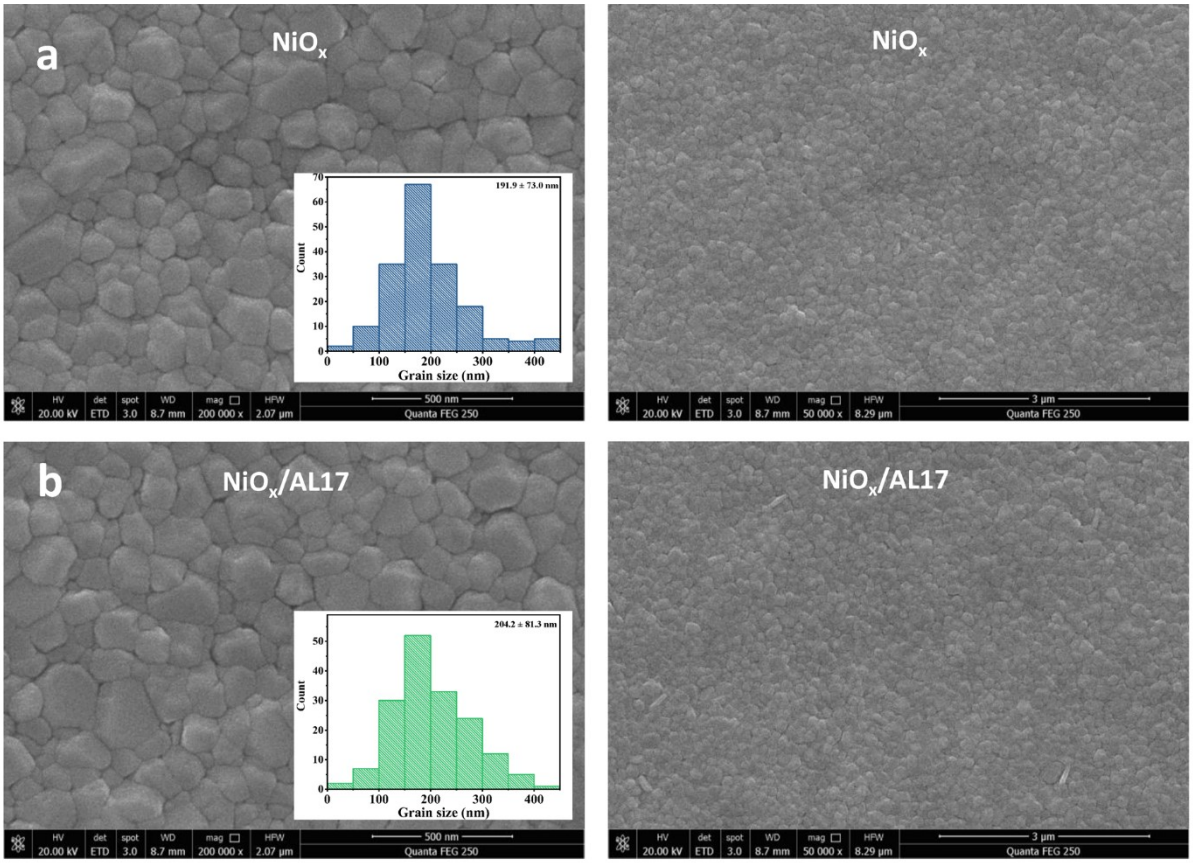

Figure S5. (a) SEM images of perovskite film deposited on NiO_x surface, with high magnification (grain size statistical histogram shown in the lower right corner) and low magnification. (b) SEM images of perovskite film deposited on NiO_x/AL17 surface, with high magnification (grain size statistical histogram shown in the lower right corner) and low magnification.

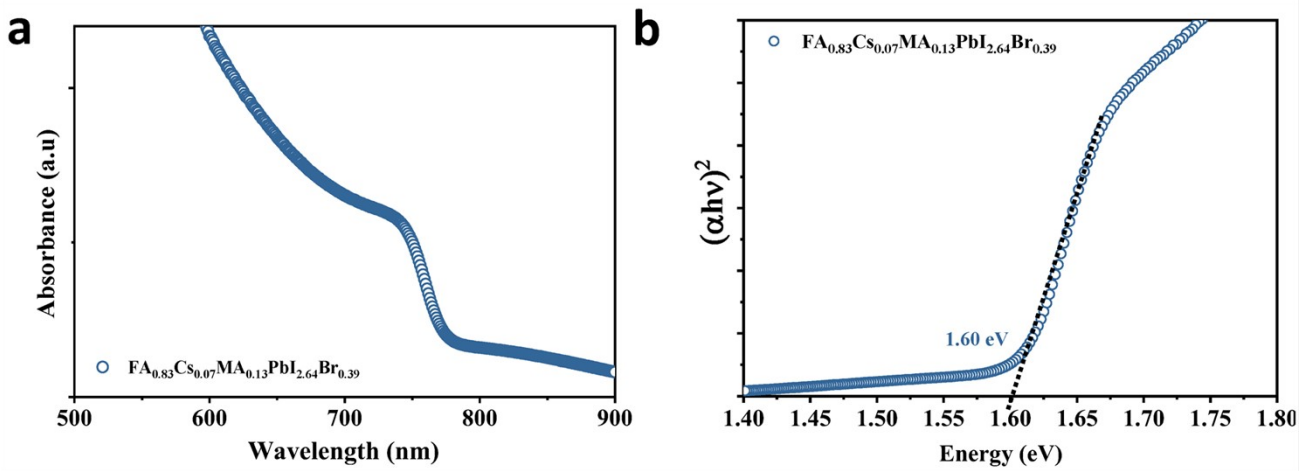

Figure S6. (a) UV-vis absorption spectrum of perovskite film. (b) $(\alpha hv)^2$-hv linear plot of perovskite film.

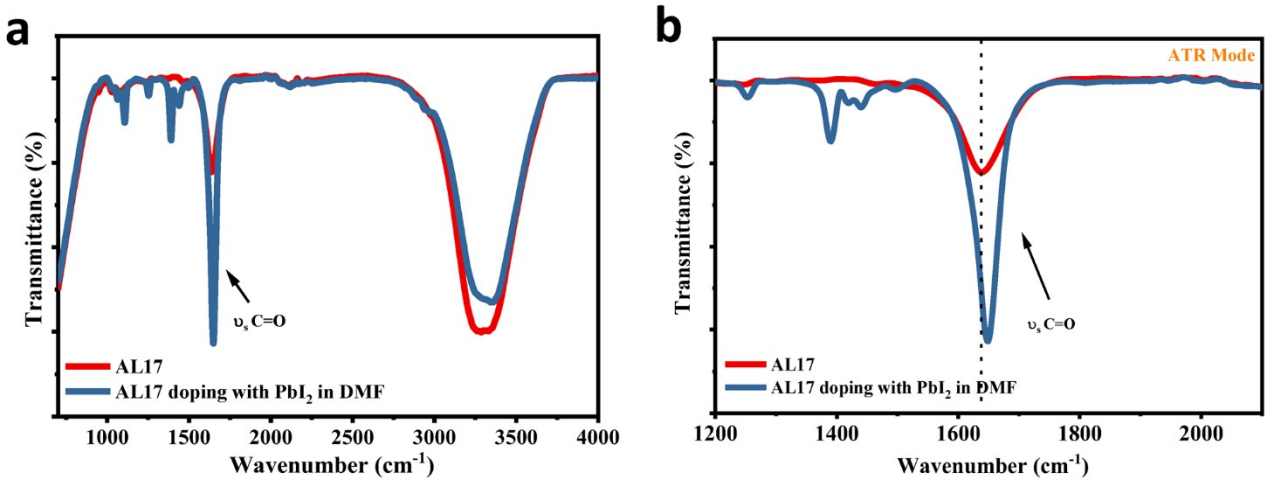

Figure S7. (a) FTIR spectra of AL17 and AL17 doping with PbI_2 in DMF by ATR mode technique. (b) The zoomed-in view of the FTIR spectrum.

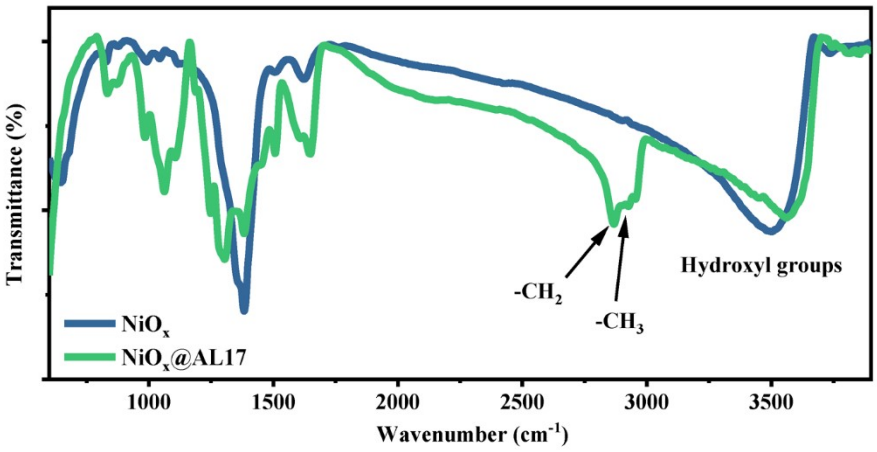

Figure S8. The full-view of the FTIR spectra of NiO_x particles and NiO_x particles coating with AL17.

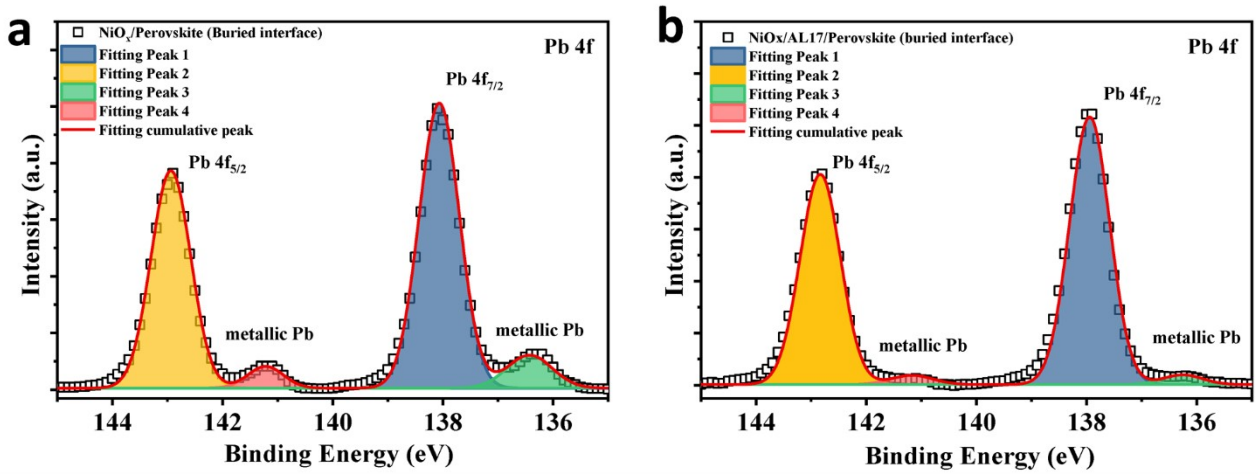

Figure S9. XPS spectra of Pb 4f core levels of the buried surfaces of NiO_x/perovskite and NiO_x/AL17/perovskite films.

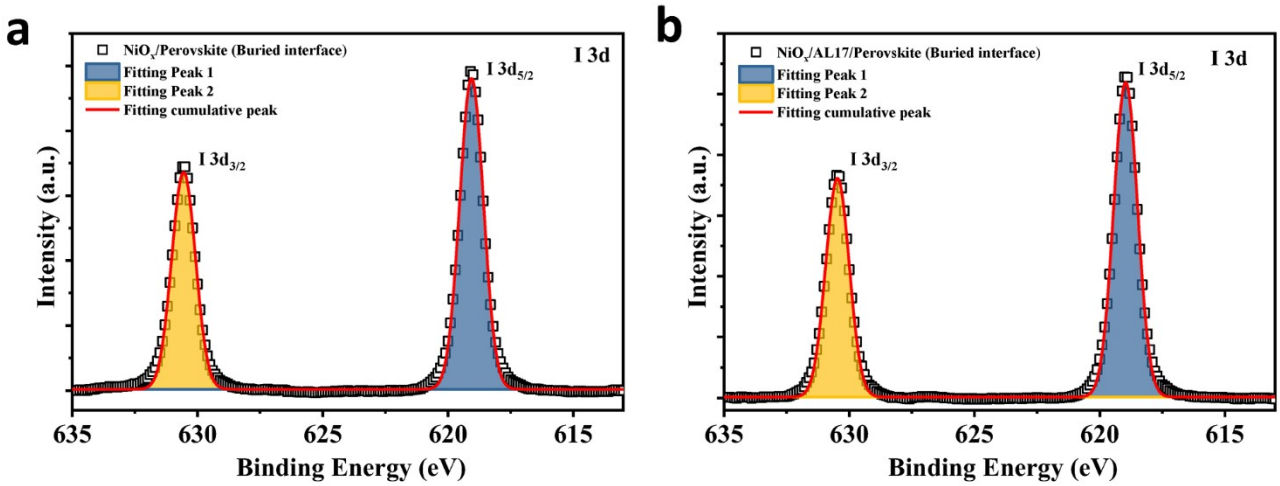

Figure S10. XPS spectra of I 3d core levels of the buried surfaces of NiO_x/perovskite and NiO_x/AL17/perovskite films.

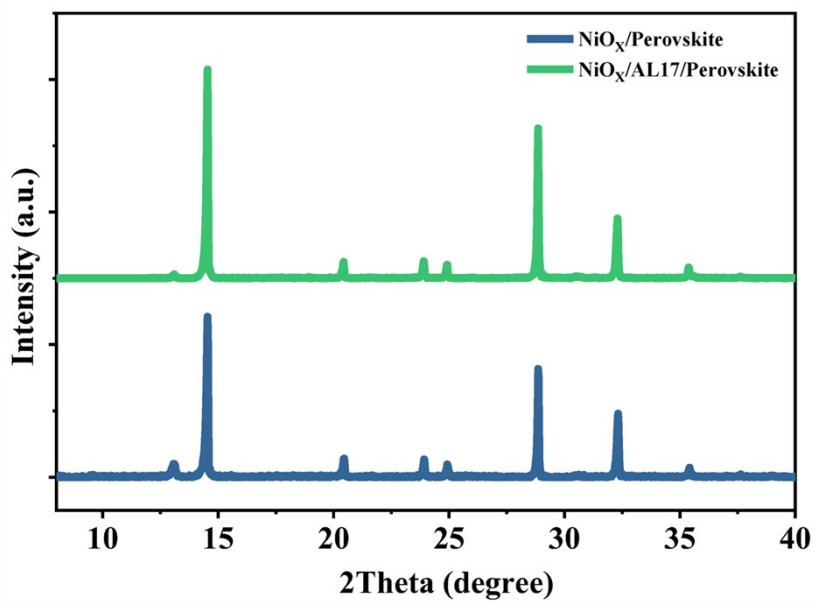

Figure S11. XRD diffraction patterns of perovskite films deposited on NiO_x and NiO_x/AL17 surfaces.

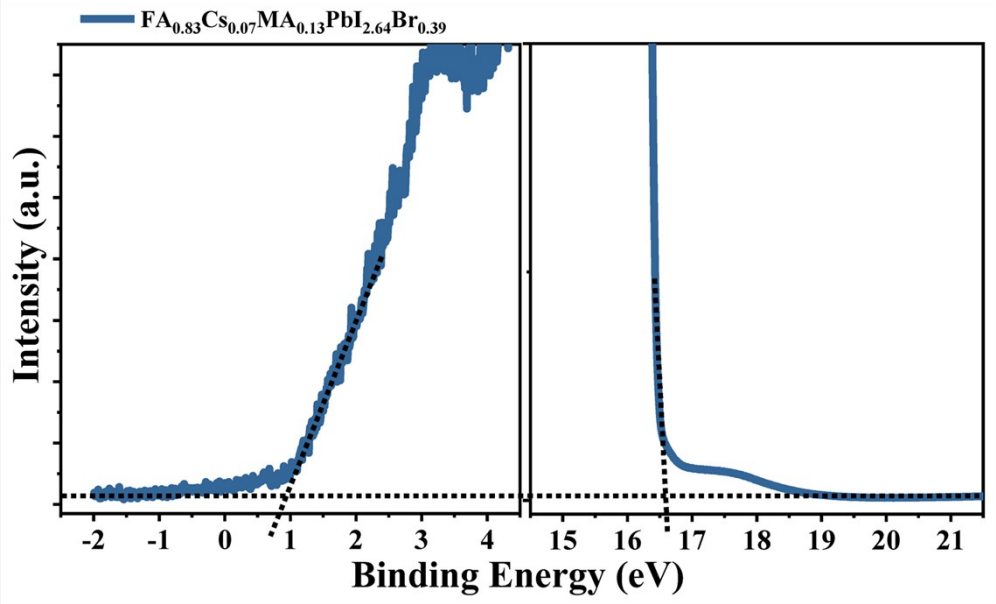

Figure S12. UPS spectrum of the perovskite film.

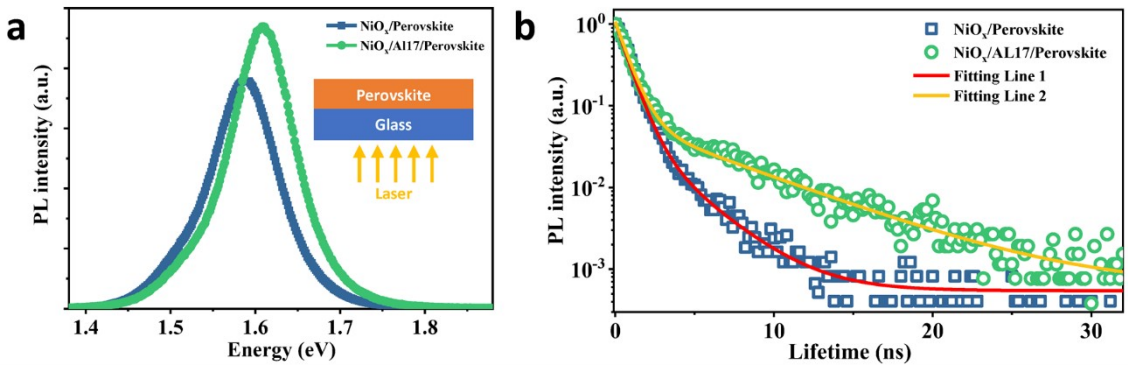

Figure S13. (a) Steady-state PL spectra of perovskite films deposited on NiO_x and NiO_x/AL17 surfaces. Excitation laser is incident from the glass side. (b) PL lifetime curves of perovskite films deposited on NiO_x and NiO_x/AL17 surfaces.

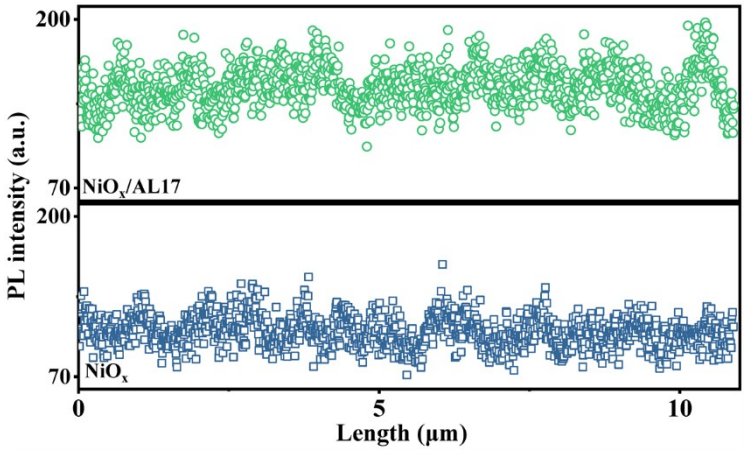

Figure S14. Fluorescence intensity curves along Line 1 and Line 2 in Figures 3f and 3g.

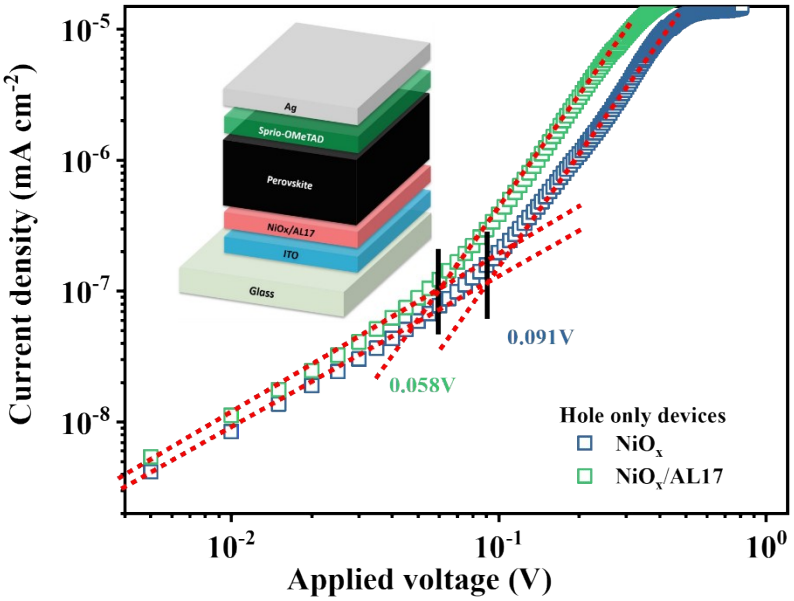

Figure S15. J-V curves of NiO_x and NiO_x/AL17-based hole-only devices.

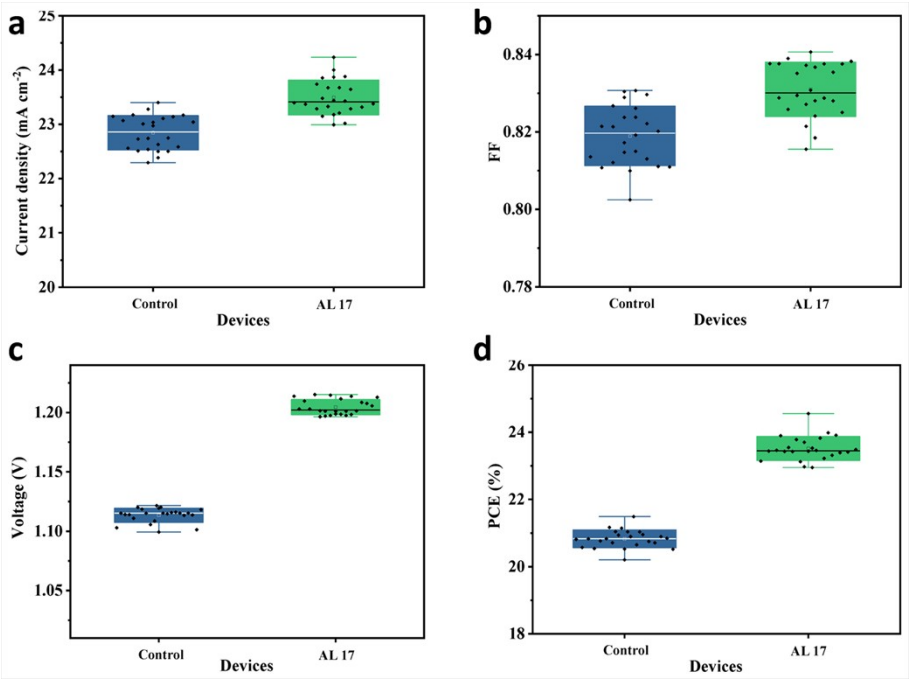

Figure S16. Statistical histograms of J_{SC}, FF, V_{OC}, and PCE for 24 control and AL17 devices.

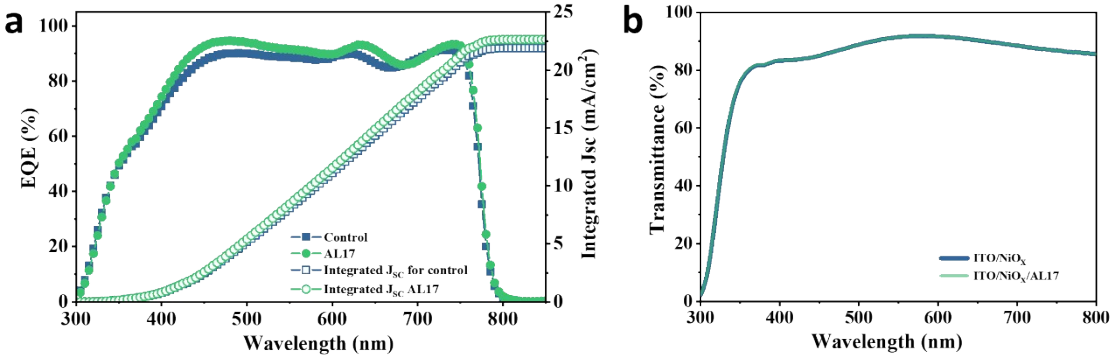

Figure S17. (a) EQE and integrated J_{SC} curves for control and AL17 devices. (b) The transmittance spectra of NiO_x and NiO_x/AL17 films.

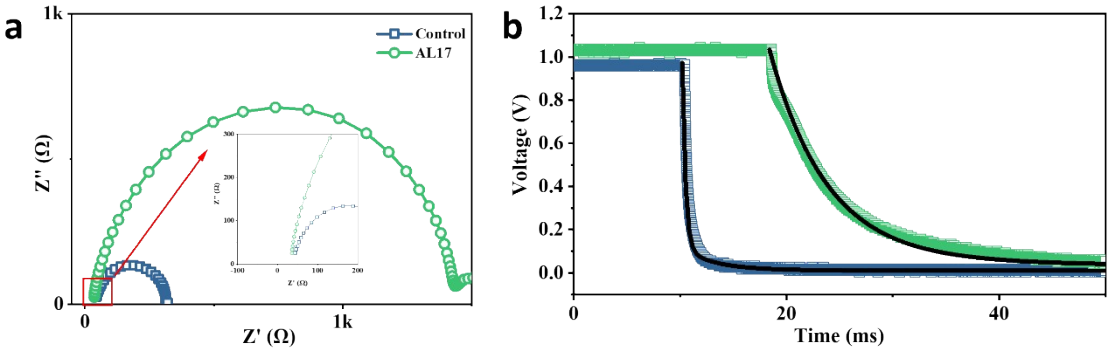

Figure S18. (a) Nyquist plots with 1.05 V applied voltage for the control and AL17 PSCs.

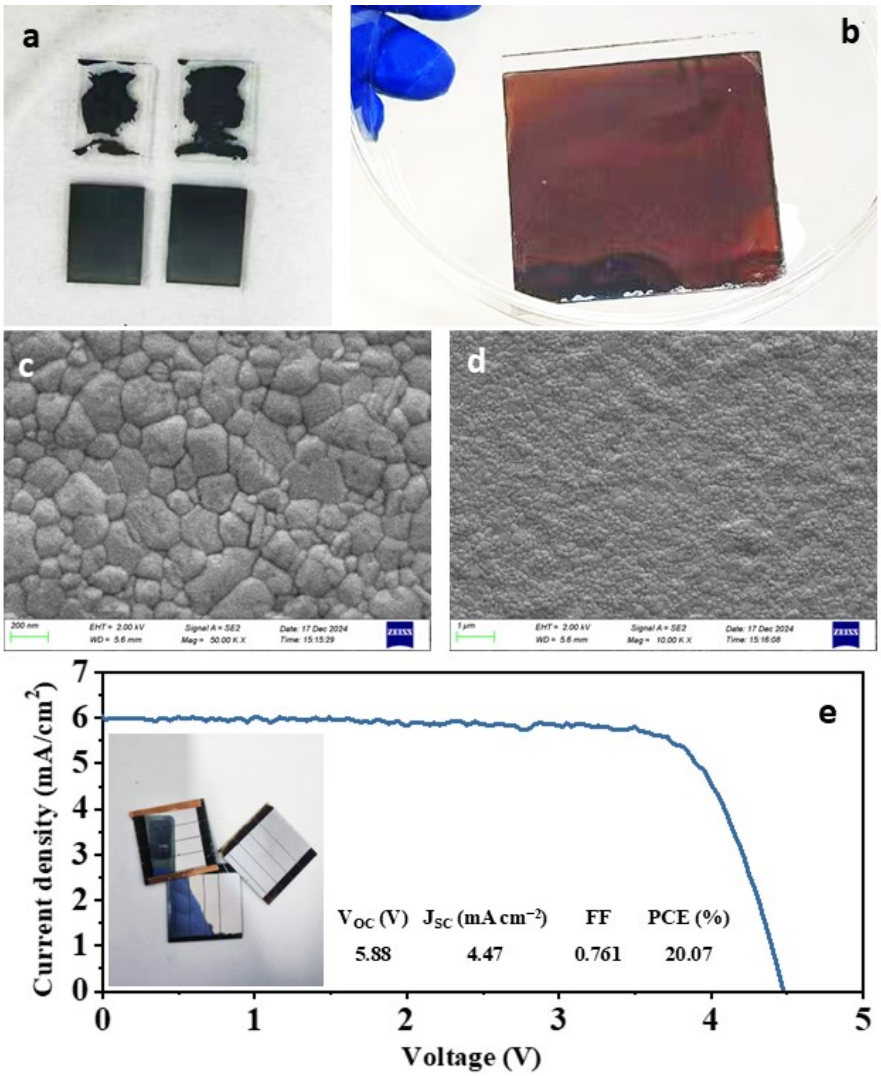

Figure S19. (a) Comparative images of perovskite films fabricated via blade-coating using hydrophobic and hydrophilic coupling agent molecules. (b) Image of a large-area perovskite film fabricated with hydrophilic coupling agent molecules via blade-coating. (c, d) Surface SEM images of blade-coated perovskite films at different magnifications. (e) J-V curve of a small-scale perovskite solar cell module fabricated by blade-coating, with an inset showing the corresponding photograph of the device.